Available online at www.sciencedirect.com
ScienceDirect
Journal of Power Sources 174 (2007) 428–434
JOURNAL OF POWER SOURCES
www.elsevier.com/locate/jpowsour

Sn–Co compound for Li-ion battery made via advanced electrospraying

M. Valvo*, U. Lafont, L. Simonin, E.M. Kelder

NanoStructured Materials, Delft Research Centre for Sustainable Energy, Delft University of Technology, Julianalaan 136, 2628 BL Delft, The Netherlands

Available online 28 June 2007

Abstract

Metallic and alloyed powders were prepared with a novel technique, called electrostatic spray reductive precipitation (ESRP). This technique combines aerosol generation by electric means together with chemical precipitation in order to form solid particles with tunable features. The structural and compositional characterizations of Co, Sn and Co–Sn materials show that metallic and alloyed nanoparticles can be obtained.

This synthesis method represents a new route to produce metal, alloyed and intermetallic particles, which here are considered as alternative anode materials for rechargeable Li-ion batteries. This approach, however, can be easily extended to the fabrication of other materials, enabling a wider range of applications e.g. for catalysis and hydrogen storage.

Keywords: Li-ion batteries; Electrospraying; Reductive Precipitation; Sn–Co; Nanoparticles

1. Introduction

During the last decade increasing attention has been paid to the synthesis of fine metals, alloys and intermetallic compounds, due to their potential use in Li-ion batteries as alternative anode materials. The request for high specific capacity, while retaining stable cyclic performance, still remains a challenge for pure elements like Sn, Sb, Si, etc., which can accept reversibly Li. Despite their high storage capacity, which is by far exceeding the one of carbonaceous materials (i.e. 372 mAh g^{-1} for graphite), the significant volume change during Li uptake and removal causes cracking and crumbling of the electrode, preventing them to be used in commercial batteries [1–5]. To minimize such detrimental effect two different approaches have been proposed: the concept of multiphase electrode [6–8] and the reduction in size of the host material [9–11]. In multiphase electrodes the active material is surrounded by an inert or non-reacting phase that acts as a "buffer," enhancing the mechanical stability of the structure during cycling. Reducing the particle size of the host material is also an effective way to decrease its absolute volume change and thus the mechanical stress, limiting the possibility of electrode cracking. Indeed, the use of nano-structured, nano-composite, or even amorphous nano-metallic hosts combined into multiphase materials has revealed a promising way to achieve improved operation capabilities [12].

In this context, investigating new synthesis methods that enable the fabrication of particles with tunable size, morphology and composition is crucial for the development of this kind of materials.

Reductive precipitation with $NaBH_4$ is a well-known technique [13,14] in materials chemistry, which has been adopted by several groups to synthesize metal, alloyed and intermetallic powders, mainly for Li-ion batteries applications. This method represents an interesting "bottom-up" alternative to the mechanical "top-down" grinding and alloying by ball-milling. The particle size and morphology of the precipitated materials can be influenced by several parameters (i.e. precursor concentrations, temperature, complexing agents, etc.) and ultrafine powders can be obtained [15]. Although reductive precipitation of metal chlorides by $NaBH_4$ is a powerful technique, which can be carried out both in aqueous and organic solutions, achieving an effective control on the particle size and size distribution often seemed to be difficult [12]. With these ideas in mind, we combined reductive precipitation (RP) with electrostatic spray pyrolysis (ESP) [16,17] of the precursors to exploit a further development for this synthesis route. Electro-spraying of liquids consists in the creation of charged aerosols by applying a high voltage between a nozzle, through which the liquid to be sprayed is fed, and a counter-electrode [18].

* Corresponding author.
E-mail address: m.valvo@tudelft.nl (M. Valvo).

0378-7753/$ – see front matter © 2007 Elsevier B.V. All rights reserved.
doi:10.1016/j.jpowsour.2007.06.156

Distinctive characteristics of this physical phenomenon are the monodispersity of the sprayed droplets, as well as the tuning of the droplet size by varying spraying parameters (i.e. flow rate, voltage, conductivity of the liquid, etc.) [19,20]. Moreover, the high net surface charge on the generated droplets causes repulsive interaction [21] and this phenomenon can prevent particle agglomeration during the reaction process, when ESP is coupled with RP. Indeed, bridging these two physical/chemical techniques enables the formation of solid nano-particles finely dispersed into a liquid medium. We called this novel process electrostatic spray reductive precipitation (ESRP).

Here, we discuss our first results for the synthesis of Co, Sn and Co–Sn particles with this technique. A comparison has been made with powders produced via RP only. Some preliminary charge–discharge curves are presented as well.

2. Experimental

Nanosized Co, Sn and Co–Sn particles were synthesized by reduction of the respective Sn^{2+}, Co^{2+} cations dissolved in the sprayed droplets of their precursor solutions. The materials used were $SnCl_2{\cdot}2H_2O$ (J.T. Baker), $CoCl_2$ (Aldrich) and $NaBH_4$ (Fluka). For the preparation of the precursor/reductive solutions we tried different solvents in order to achieve an efficient coupling of the spraying process with reductive precipitation. No complexing agents were added in our experiments.

Solutions with low precursor concentrations (0.05, 0.1 M) were prepared for the spray. We did not use water as solvent for the whole process because its electrical conductivity is too high and therefore hinders stable electro-spraying. Instead, organic solvents like di-methyl sulfoxide (DMSO) or isopropyl alcohol (IPA) were preferred, which show also high stability towards $NaBH_4$. For the syntheses each time 30 wt% excess of $NaBH_4$ was added to the calculated stoichiometric amount to ensure complete reduction of the precursors. Both precursor and reductive solutions were separately prepared, sealed and stirred overnight before starting the experiments. The experiments were carried out in air at room temperature (RT). A syringe pump (Kd Scientific model 100 series) and a 10 ml glass syringe (Fortuna Optima) were used to inject the precursor solution through the electrified nozzle (EFD Ultra, Ø 0.25 mm) with a constant flow rate. Typically, low flow rates (i.e. 1.5 ml h^{-1}) were employed. A high voltage supply (HCN 14-12500, FUG) was used to apply a high voltage (i.e. $0 \div 12.5$ kV) between the nozzle and the counter-electrode in order to generate the precursor aerosol.

Under the influence of the electric field small charged droplets are formed and attracted towards a ring, which is placed in the reductive solution. In this way, the droplets containing the precursor metal ions are driven into the reductive bath, where they are immediately reduced to the metallic, alloy or intermetallic state. A simplified scheme of the experimental set up is shown in Fig. 1.

The general reactions employed here to form pure metallic particles (1) or different metallic compositions (2) are the following:

$$MCl_x + x \cdot NaBH_4 \rightarrow M_{\downarrow} + x \cdot NaCl + x \cdot BH_3^{\uparrow} + \left(\frac{x}{2}\right) \cdot H_2^{\uparrow} \quad (1)$$

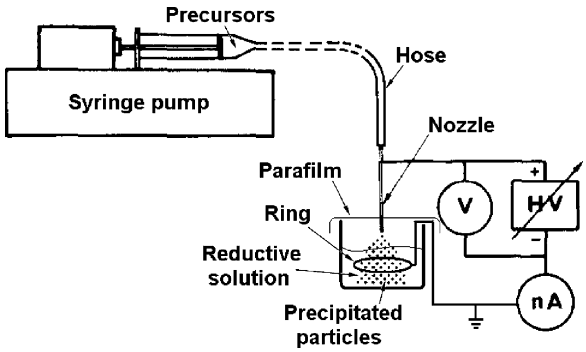

Fig. 1. Scheme of the ESRP set up.

$$X \cdot MCl_x + Y \cdot M'Cl_y + (Xx + Yy) \cdot NaBH_4 \rightarrow (M_X M'_Y)_{\downarrow} + (Xx + Yy) \cdot NaCl + (Xx + Yy) \cdot BH_3^{\uparrow} + \left(\frac{(Xx + Yy)}{2}\right) \cdot H_2^{\uparrow} \quad (2)$$

where M and M′ refer to metal ions. For the synthesis of pure Sn or Co by reaction (1) $x = 2$, while for intermetallic $CoSn_2$ we have reaction (2) where $x = 2$, $y = 2$, $X = 1$ and $Y = 2$. It should be noted, however, that this process still suffers from the presence of unwanted reaction by-products (i.e. NaCl), which need to be washed off.

The suspension obtained after the reaction was stirred for about 20 min and then centrifugation was carried out to separate the powders from the liquid. The powders then were carefully washed several times with ethanol and water, rinsed with acetone and finally dried and stored under vacuum at RT.

The morphology, size, crystallinity and composition of the particles were investigated by a Philips CM30T transmission electron microscope (TEM) operated at 300 kV, equipped with a LINK EDX probe (Oxford). Besides, the collected powders were analyzed by a Philips XL20 Scanning Electron Microscope (SEM) and a Bruker (AXS D8 advance) X-ray diffractometer, with a Cu–K_α radiation source for XRD. Angular scans were recorded between 10° and 90° with a scan speed of 0.1° min^{-1}.

Electrochemical measurements were performed with Swagelok cells assembled inside a He-filled glove box. The dry powders were mixed with 20 wt% carbon black (Alfa) and inserted into the cell, having lithium as counter and reference electrode. A 1 M $LiPF_6$ solution in ethylene carbonate, ethyl-methyl carbonate, dimethylene carbonate, EC:EMC:DMC 1:2:2 was used as electrolyte. The galvanostatic tests were carried out with a Maccor (S-4000) cycler between 0 and 2 V, with a constant gravimetric current density of about 45 mA g^{-1}.

3. Results and discussion

Initially, we synthesized tin particles without applying any voltage to check the typical size of the materials that can be produced via reductive precipitation only. For this purpose, we simply used a drop-wise addition of the Sn precursor solution, controlled by the syringe pump (1.5 ml h^{-1}). Fig. 2 shows the TEM images of the dried powders.

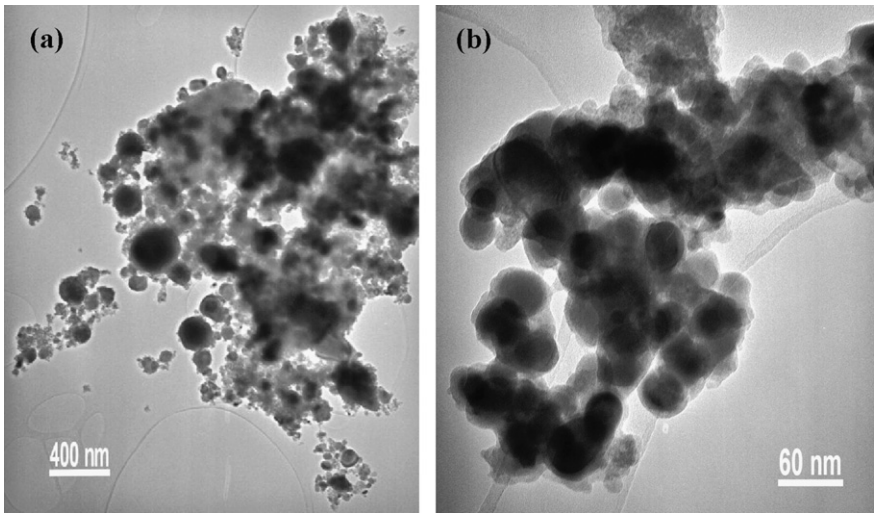

Fig. 2. TEM micrographs of tin powders produced by precipitation only with $NaBH_4$. $SnCl_2$ solution (0.1 M) in IPA was used as liquid precursor.

It is clearly visible from Fig. 2(a) that the powders of the precipitated material are strongly agglomerated and not homogeneous in size. Furthermore, the primary particles are spherical and have sizes in the range of 30–300 nm.XRD analysis of the same sample is presented in Fig. 3. From the spectrum it is seen that the powders consist of crystalline tin. No crystalline impurities related to the reaction by-products or to the excess of $NaBH_4$ were detected. Furthermore, no crystalline peaks associated to tin oxides (i.e. SnO and SnO_2) were found. However, it should be stressed that the presence of amorphous oxide compounds or impurities could not be excluded, particularly tin oxides, because the collected powders have been exposed to air and have not undergone any thermal treatment under other reductive conditions.

Subsequently, we applied an electric field to the dripping nozzle in order to obtain an electro-spray of the same Sn precursor solution, under identical experimental conditions. As it was expected, the use of the high voltage caused a clear change in the structure of the synthesised materials. Fig. 4 depicts a SEM image of the powders obtained by ESRP at 2 kV.

From the SEM picture it can be seen that the sample exhibits a large surface area, and that the particle size distribution is quite narrow. All the particles are spherically-shaped and loosely agglomerated. The typical particle size is estimated around 40–50 nm. For analysing these particles in more detail TEM has been employed. In Fig. 5 the TEM images of the same sample are shown.

The powders exhibited a flocky morphology (Fig. 5(a)). Even though agglomeration is encountered through the sample, the particle size distribution is quite uniform, and big particles are not observed in this case. It can also be noted from Fig. 5(b) that the primary particles are small spheres of few nanometres. They are densely packed in these fluffy agglomerates, but still discernible. Moreover, a careful inspection of Fig. 5(b) reveals the presence of several nano-crystalline domains (magnified inset).

The results of the XRD analysis carried out on the same powders are shown in Fig. 6. Also in this case, XRD confirmed the presence of peaks associated to crystalline Sn. However, the recorded pattern is clearly very different from the one depicted in Fig. 3.

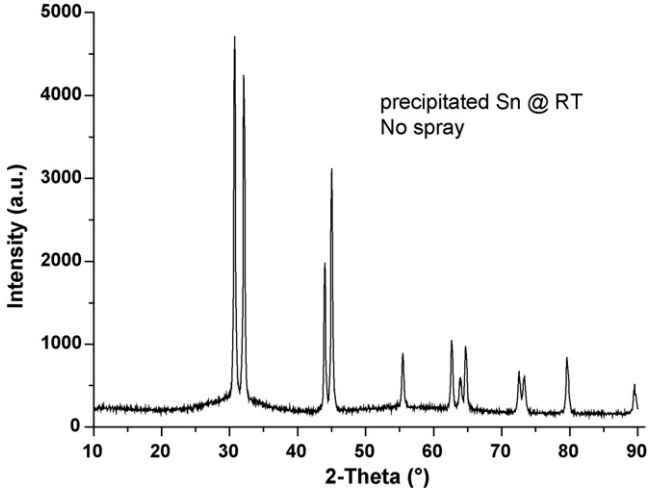

Fig. 3. XRD pattern of Sn powders synthesized via RP.

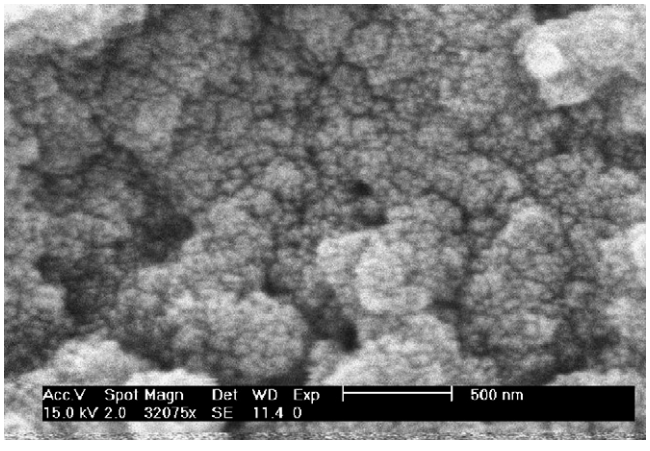

Fig. 4. SEM image of Sn powders obtained by ESRP at 2 kV. Note the homogeneously-sized, rounded particles.

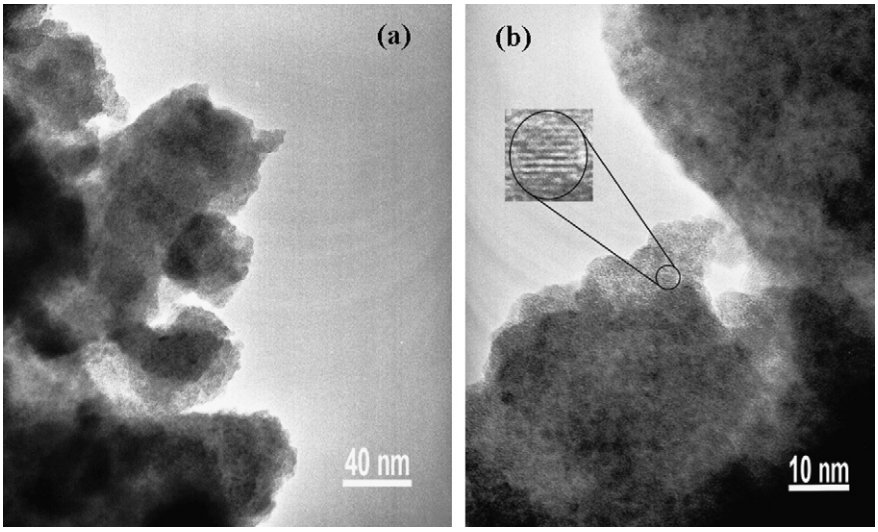

Fig. 5. TEM micrographs of Sn powders produced by ESRP applying a voltage of 2 kV.

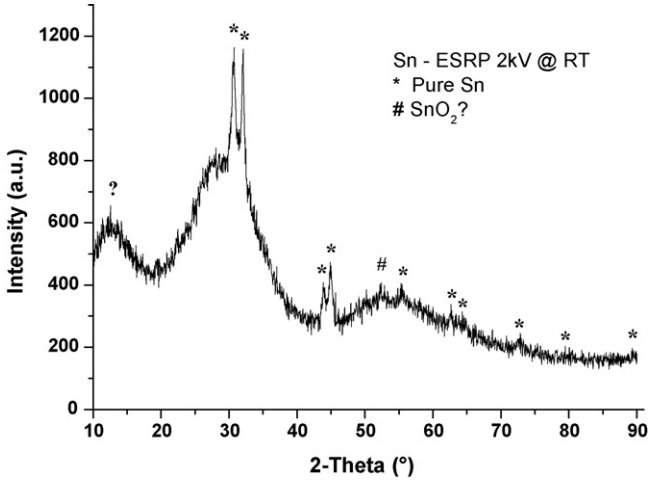

Fig. 6. XRD spectrum of Sn powders obtained by ESRP at 2 kV. Note the big humps around 12°, 30° and 55°.

In particular, the intensity of all the characteristic Sn peaks is reduced, while their respective signals are broadened. These are typical features related to the presence of nanoparticles. Moreover, the XRD pattern is characterized by broad humps centred around 12°, 30° and 55°. The crystalline peaks are somehow superimposed on these "amorphous humps" and the less intense Sn lines are not readily distinguishable. The origin of these humps still remains unclear, but it is probably due to the sample processing (i.e. air exposure) and similar features have been reported earlier [22]. In any case, an enhanced amorphization of the collected powders has been observed. Decreasing the particle size results in increasing the contribution of surface atoms and that makes nanopowders more reactive than their bulk counterparts. Therefore, surface amorphous oxides/contaminants, which are likely to form/deposit in contact with air during the sample processing, should have more and more influence on the materials. However, it should also be mentioned that in this case no crystalline impurities were clearly detected.

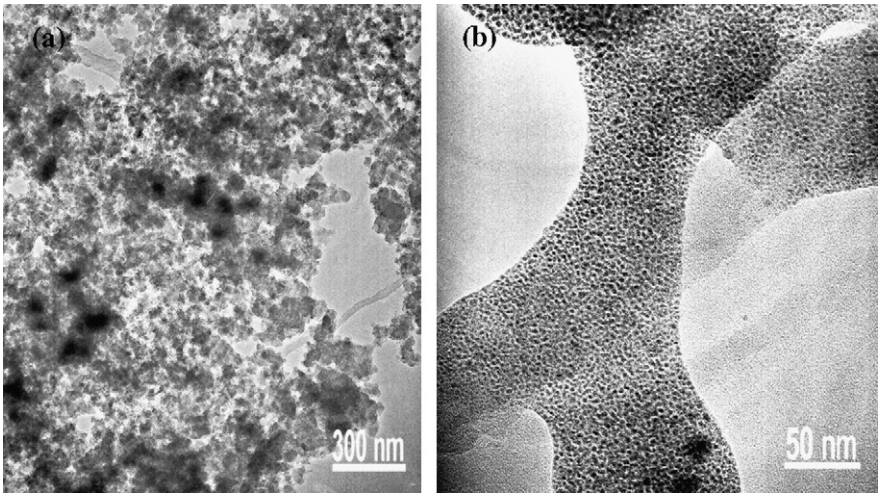

Fig. 7. TEM micrographs of "as-produced" Co particles by ESRP at 9 kV in IPA.

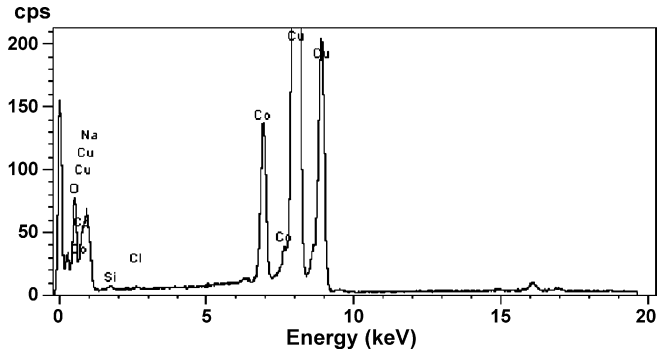

Fig. 8. EDX spectrum of Co particles produced by ESRP at 9 kV in IPA. The intense Cu lines are due to the copper grid of the sample holder.

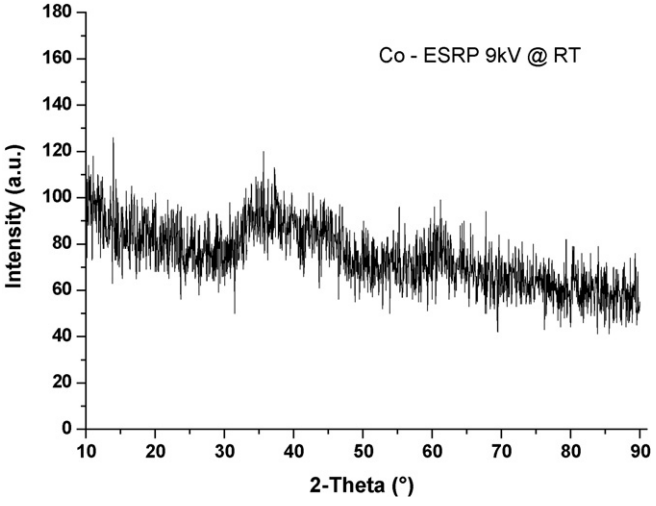

Fig. 9. XRD pattern of Co particles synthesized at 9 kV in IPA.

To have a better understanding of the nature and the structure of the materials that can be synthesized via ESRP, "as-produced" particles before being centrifuged and washed were studied. In that respect, Co particles were synthesized by applying 9 kV and an injection flow rate of 1.5 ml h^{-1}. A precursor solution of $CoCl_2$ 0.1 M in IPA was used for this purpose. Fig. 7 depicts two TEM images of the as-produced materials.

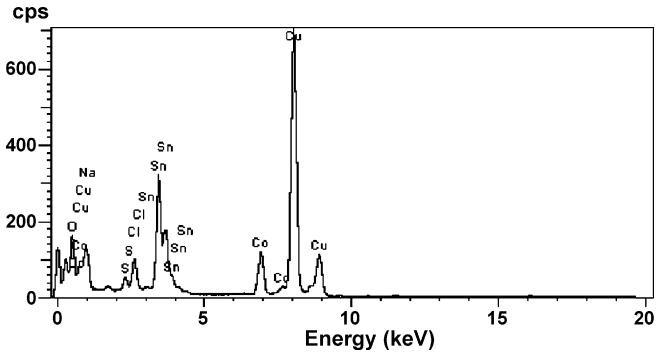

Fig. 11. EDX spectrum of Co–Sn particles synthesized by ESRP. Note the presence of other elements associated to the reaction by-products and to the used solvent.

Fig. 7(a) shows the overall picture of the sample and a certain tendency towards particle agglomeration can be seen. However, the image taken at higher magnification (Fig. 7(b)) reveals that very small particles have been formed. They are dispersed in a sort of "matrix," in which they are densely packed. Still the particles appear clearly separated from each other. Again, the particles exhibited a spherical shape and their average size is around 2–5 nm.

The local composition was investigated by EDX (Fig. 8), which demonstrated the presence of other elements associated to the reaction by-products (i.e. NaCl) and to the TEM sample preparation (i.e. Si, O).

Moreover, the synthesized particles proved to be amorphous, as confirmed by XRD analysis (Fig. 9).

Finally, we tried to produce particles with Co–Sn composition. We used $CoCl_2$ and $SnCl_2$ (0.05 M: 0.1 M) in DMSO as precursor solution to form $CoSn_2$ compound.

Irrespective of the difference in the solvent and the precursors concentration, the as-produced particles (Fig. 10) displayed similar characteristics to the ones represented in Fig. 7.

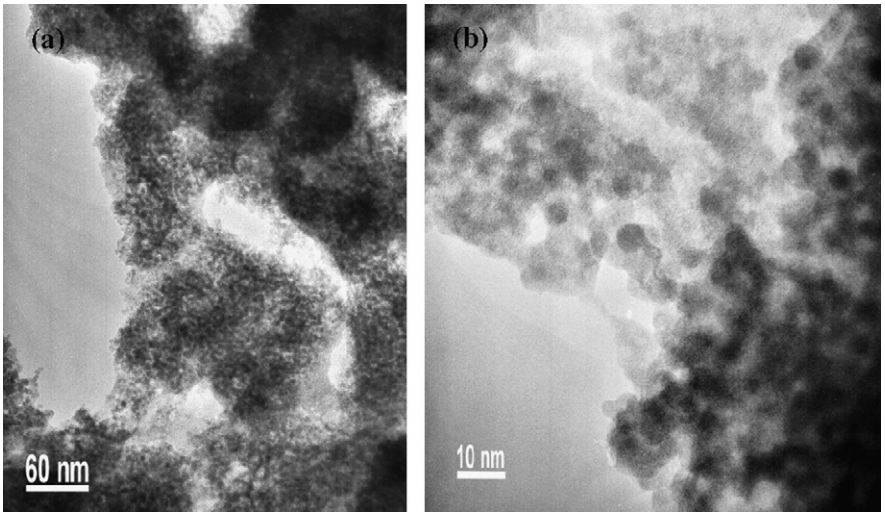

Fig. 10. TEM micrographs of "as-produced" Co–Sn particles by ESRP (9 kV, 1.5 ml h^{-1}) in DMSO.

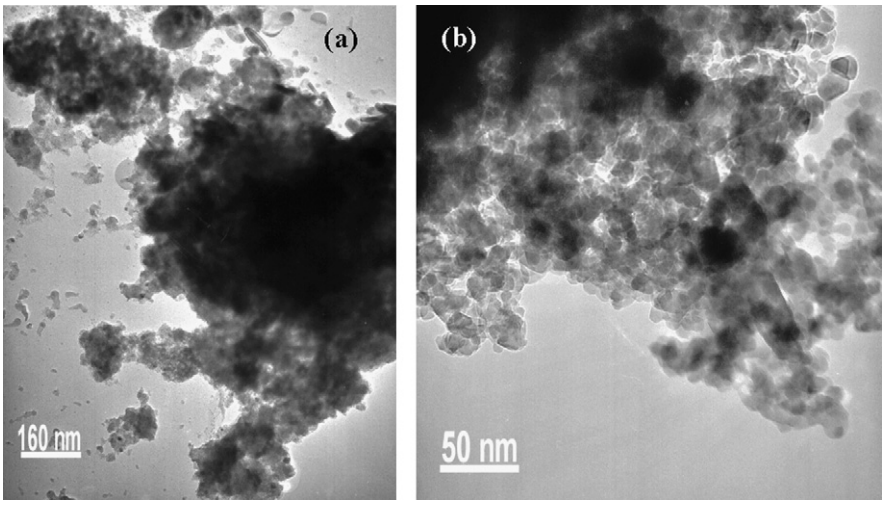

Fig. 12. TEM images of the collected Co–Sn powders synthesized by ESRP at 9 kV.

In Fig. 10 it can be seen that there are certain agglomerates, but clearly the primary particle size is below 10 nm and are merely amorphous.

The results of the elemental analysis carried out on the same sample are presented in Fig. 11.

Peaks associated to Sn and Co are distinguishable and their integrated signals are roughly in accordance with the stoichiometry as expected for the $CoSn_2$ compound. Nevertheless, it cannot be excluded that the stoichiometry may vary throughout the sample so as to form locally different compositions.

The same sample was also investigated after centrifugation, washing and drying to check the influence of these post-synthesis processing's on the structure of the final materials. The results of the TEM analysis are shown in Fig. 12.

It is clear from Fig. 12(a) that the morphology of the collected powders is strongly influenced by the post-synthesis treatments, which cause further agglomeration of the particles.

Despite these detrimental effects, it can be observed from Fig. 12(b) that the primary particles retained substantially their structure, and only few bigger agglomerates were detected.

Finally, a XRD analysis of the collected materials was carried out (Fig. 13), followed by an electrochemical test.

Also in this case the observed XRD pattern revealed an amorphous character for the powders and no crystalline peaks were

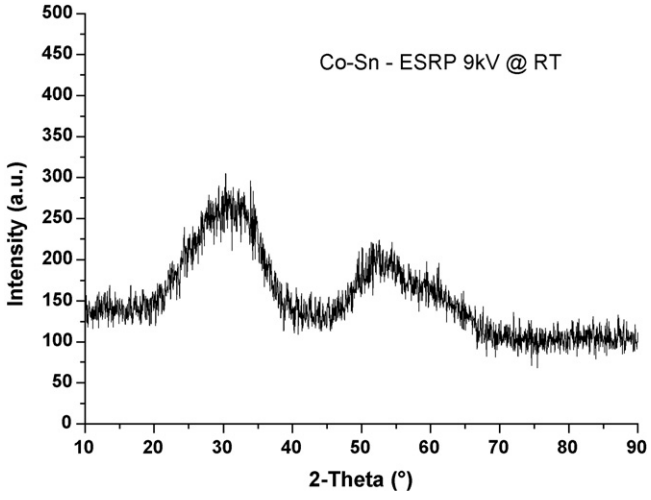

Fig. 13. XRD pattern of Co–Sn powders.

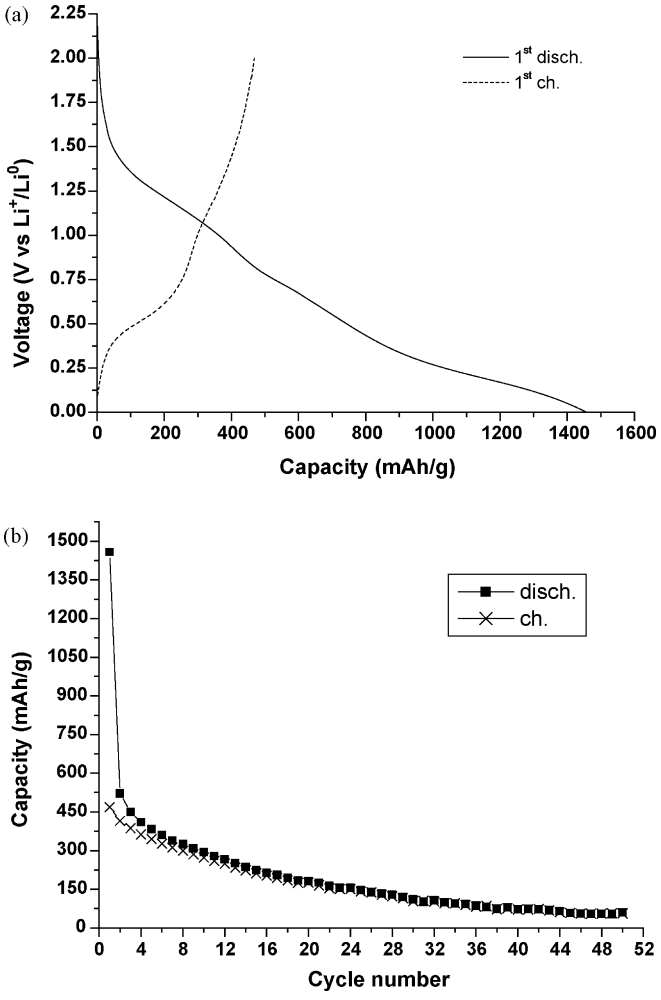

Fig. 14. (a) Preliminary charge–discharge curves of Co–Sn powders; (b) cyclic performance.

observed. Again, the presence of amorphous oxides cannot be excluded.

The results of the electrochemical tests are shown in Fig. 14.

In Fig. 14(a) a large irreversible capacity is observed in the first cycle. Despite the considerable value of the initial discharge capacity, only one third of it is recovered during the first charge. This circumstance is likely due to the fact that the powders produced via the spray process show large surface area. In that respect, the presence of oxides and impurities is detrimental for their electrochemical behaviour, being responsible for capacity loss, especially during the first cycle. The "sloping shape" of the charge–discharge curves, which do not exhibit distinct plateaus, also confirms the amorphous nature of the small particles in the analyzed powders. Indeed, flat plateaus indicate phase separation during Li alloying and are normally related to particles characterized by relatively large size and good crystallinity [12].

Nanosized amorphous metal particles are expected to enhance capacity retention upon cycling. However, in our case the features of the cyclic performance (Fig. 14(b)) show a clear fading in the capacity retention. This circumstance can be explained taking into account a more or less pronounced oxidation of the nanoparticles during the washing and the final collection procedures.

Improving the purity of the produced particles is not a trivial task, since they proved to react readily with oxygen. This will be one of the first goals for future research.

4. Conclusion

Initial results show that ESRP is a promising technique for the synthesis of metallic, alloyed and metallic-like nanoparticles. Primary particle sizes in the range of 2–5 nm can be achieved by proper selection of the process parameters. A careful investigation has started as a basis for studying a wide range of materials that can be used for other applications (e.g. catalysis, hydrogen storage).

Acknowledgements

The authors would like to acknowledge the Delft Research Centre for Sustainable Energy SENECU, the European Network of Excellence ALISTORE, and the Dutch Ministry for Economic Affairs via SenterNovem and STW for funding the programme for nanomaterials syntheses.

References

[1] J. Yang, M. Wachtler, M. Winter, J.O. Besenhard, Electrochem. Sol. State Lett. 2 (1999) 161.
[2] J. Yang, Y. Takeda, N. Imanishi, J.Y. Xie, O. Yamamoto, Solid State Ionics 133 (2000) 189.
[3] H. Mukaibo, T. Osaka, P. Reale, S. Panero, B. Scrosati, M. Wachtler, J. Power Sources 132 (2004) 225.
[4] N. Pereira, L.C. Klein, G.G. Amatucci, Solid State Ionics 167 (2004) 29.
[5] S.A. Needham, G.X. Wang, H.K. Liu, J. Alloys Compounds 400 (2005) 234.
[6] B.A. Boukamp, R.A. Huggins, J. Electrochem. Soc. 128 (1981) 725.
[7] Y. Idota, T. Kubota, A. Matsufuji, Y. Maekawa, T. Miyasaka, Science 276 (1997) 1395.
[8] M. Winter, J.O. Besenhard, M.E. Spahr, P. Novak, Adv. Mater. 10 (1998) 725.
[9] J. Yang, M. Winter, J.O. Besenhard, Solid State Ionics 90 (1996) 281.
[10] A.H. Whitehead, J.M. Elliott, J.R. Owen, J. Power Sources 81 (1999) 33.
[11] H. Li, X.J. Huang, L.Q. Chen, Z.G. Wu, Y. Liang, Electrochem. Sol. State Lett. 2 (1999) 547.
[12] A. Trifonova, M. Wachtler, M.R. Wagner, H. Schroettner, Ch. Mitterbauer, F. Hofer, K.C. Möller, M. Winter, J.O. Besenhard, Solid State Ionics 168 (2004) 51.
[13] H.I. Schlesinger, H.C. Brown, A.E. Finholt, J.R. Gilbreath, H.R. Hoekstra, E.K. Hyde, J. Am. Chem. Soc. 75 (1953) 215.
[14] L. Zhang, A. Manthiram, J. Mater. Chem. 6 (1996) 999.
[15] M. Wachtler, M. Winter, J.O. Besenhard, J. Power Sources 105 (2002) 151.
[16] A.A. van Zomeren, E.M. Kelder, J.C.M. Marijnissen, J. Schoonman, J. Aerosol Sci. 25 (1994) 1229.
[17] E.M. Kelder, O.C.J. Nijs, J. Schoonman, Solid State Ionics 68 (1994) 5.
[18] M. Cloupeau, J. Aerosol Sci. 25 (1994) 1143.
[19] G.M.H. Meesters, P.H.W. Vercoulen, J.C.M. Marijnissen, B. Scarlett, J. Aerosol Sci. 23 (1992) 37.
[20] J. Fernandez de la Mora, J. Navascues, F. Fernandez, J. Rossell-Llompart, J. Aerosol Sci. 21 (1990) S673.
[21] A.M. Gañán-Calvo, J. Dávila, A. Barrero, J. Aerosol Sci. 28 (1997) 249.
[22] Q.F. Dong, C.Z. Wu, M.G. Jin, Z.C. Huang, M.S. Zheng, J.K. You, Z.G. Lin, Solid State Ionics 167 (2004) 49.